Colossal permittivity, impedance analysis and electric properties in AlGaN/GaN HEMTs

H. Mosbahi[a], A. Essaoudi[b], N. E. Gorji[c], A. Gassoumi[d*], A. Almohammedi[e], A. Helali[f], M. Gassoumi[b]

[a] *Department of Transport Technology and Engineering, Higher Institute of Transport and Logistics, University of Sousse, Tunis*[b]*Laboratory of Condensed Matter and Nanosciences, University of Monastir, Monastir 5000, Tunisia*

[c]*Mechatronic Engineering, Technological University Dublin, Dublin 15, Ireland*

[d]*Department of Physics, Faculty of Science, King Khalid University, P.O. Box 9004, Abha, 61413, Saudi Arabia*

[e]*Department of Physics, Faculty of Science, Islamic University of Madinah, Madinah, 42351, Saudi Arabia*

[f]*Laboratory of Micro-Optoelectronics and Nanostructures (LMON), University of Monastir, Avenue of the Environment, 5019 Monastir, Tunisia*

The electric and dielectric processes of AlGaN/GaN/Si HEMTs produced by molecular beam epitaxy were examined utilizing direct current-voltage, impedance spectroscopy, and DLTS measurements. Using current-voltage measurements, the DC electrical characteristics of AlGaN/GaN/Si HEMTs revealed the self-heating effect. The relaxation dynamics of charge carriers appear to be studied by the conductance mechanism and electric modulus formalisms. Behavior that is frequency dependent has been observed in impedance spectroscopy. Last but not least, DLTS data have demonstrated the existence of electron traps. The prevalence of parasitic effects and conduction mechanisms are remarkably correlated with deep levels.

(Received October 22, 2023; Accepted December 13, 2023)

Keywords: AlGaN/GaN/Si HEMTs, DC measurements, Conductance, Impedance spectroscopy, Dielectric measurements, Electron trap, DLTS

1. Introduction

AlGaN/GaN high electron mobility transistors (HEMTs) have drawn lots of attention for high-frequency and high-power applications [1-4]. Nitride based materials feature properties such as wide band gaps, large breakdown bias voltage, high saturation velocity, high electron mobility, high efficient carrier transport as well as a wurtzite material [5]. A two-dimensional electron gas (2DEG) in AlGaN/GaN heterointerface results from high carrier density due to the effect of strong spontaneous and piezoelectric polarization fields [6]. Silicon, sapphire and silicon carbide are the substrates on which the nitride layer are grown [7,8]. These substrates determines the crystalline quality of the layers and leads to high dislocation densities [9]. By optimizing the growth condition and design parameters, performance of AlGaN/GaN heterostructure transistors have been improved [6, 10-12]. Encouraging results were obtained in this research field.

Reliability limitation of HEMTs AlGaN/GaN has primarily focused on impurities and defects. Know reliability issues for HEMTs AlGaN/GaN are parasitic effects due to current collapse, self-heating, kink effect, leakage current, gate-lag, drain-lag as well as traps in devices [13-17]. The origin of the parasitic effects were characterized by different techniques. The techniques are current-voltage measurements, capacitance-voltage characteristics, pulse measurements, deep level transient spectroscopy, Fourier transform deep-level transient spectroscopy, conductance deep level transient spectroscopy and impedance spectroscopy

* Corresponding author: abdelaziz.gassoumi@gmail.com
https://doi.org/10.15251/JOR.2023.196.763

[9,17,18-22]. To overcome limitations of the AlGaN/GaN HEMTs reliability, a considerable progress has continued the study of these heterostructures to reduce parasitic effects.

In the present work, we described the electrical properties, conductance mechanism, relaxation process and DLTS measurements of AlGaN/GaN/Si HEMTs. For the same HEMT structures, we have also discussed the electrical characteristics required by impedance spectroscopy, showing low acquired dielectric loss. Results has been correlated in order to explain the origin of the electron transport.

2. Background

2.1. Electrical and dielectric measurements

Electrical behavior of the devices can be described by different techniques such as DC measurements, impedance spectroscopy and DLTS. Impedance spectroscopy can be expressed by various parameters as follows:

Complex impedance:

$$Z(w) = Z'(w) + j\,Z''(w) \tag{1}$$

Complex modulus:

$$M(w) = M'(w) + j\,M''(w) \tag{2}$$

Complex permittivity:

$$\varepsilon(w) = \varepsilon'(w) + j\,\varepsilon''(w) \tag{3}$$

Tangent loss:

$$tg(\delta) = \frac{\varepsilon''(\omega)}{\varepsilon'(\omega)} \tag{4}$$

with $w = 2\,\pi\,f$

where f is the frequency.

Impedance spectroscopy measurements were performed using a HP4192 LF impedance analyser. The conductance characteristic were recorded from the excitation potential for ac measurements. The DC measurements is carried out by Hewlett Packard 41428 Modular. Experimental data were made in the dark at atmospheric pressure.

DLTS is a technique to characterize the defects in AlGaN/GaN/Si HEMTs. DLTS measurements were realized using a PAR 410 capacitance meter lock-in detection.

2.2. Experimental

The AlGaN/GaN HEMTs under investigation are grown on silicon (111) substrate by using molecular beam epitaxy (MBE). The active layers consist in a 500 nm thick of undoped AlN/AlGaN buffer, a 1.8 µm undoped GaN channel, a 23 nm thick of undoped $Al_{0.26}Ga_{0.74}N$ barrier and a 1 nm n^+- GaN cap layer. The ohmic contact pads are patterned using e-beam lithography. Hereafter, the metallization by means of evaporated 12/200/40/100 nm Ti/Al/Ni/Au is deposited at 900°C during 30s. The Schottky gate is realized using 100/150 nm Mo/Au layers.

3. Direct-current characteristics

Direct-current measurements have been performed on AlGaN/GaN/Si HEMTs at room temperature. Fig. 1 shows the drain–source current as a function of drain-source voltage at different V_{gs}. It is found that the maximum of drain-source current is 0.22 A. However, the

saturation current exhibits a negative conductance at large drain-source voltage. It is worth noticing that this behavior is due to the self-heating. It can be seen that the self-heating results from a increase in the local temperature of 2DEG, a decrease in the electron mobility and trapping centers in heterointerface [17].

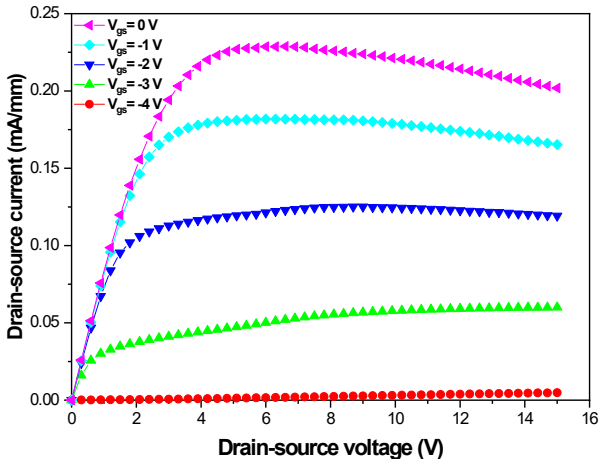

Fig. 1. Direct-current characteristics of the AlGaN/GaN/Si HEMTs devices at different bias voltages.

Electron transport parameters are summarized in Table 1. The transconductance (g_m) and the threshold voltage shift (V_{th}) have been revealed from the relevant drain-source current as function gate-source current I_{ds}-V_{gs} plots. These parameters are assigned to the electron sheet concentration in the 2DEG conductive. The barrier height (V_b) and the ideality factor (η), have deduced from the gate leakage current I_{gs}-V_{gs}, an attempt to analyze the quality of Schottky contact [17-18]. It can be seen that these parameters evaluated the performance and transport properties of AlGaN/GaN/Si HEMTs.

Table 1. Electron transport parameters of the AlGaN/GaN/Si HEMT.

I_{ds} (A)	g_m (mS/mm)	V_{th} (V)	η	V_b (V)	R_s+R_i (Ω)
0.22	210	-4.1	1.01	0.78	4.2

4. Electrical conductance analysis

To avoid the charge transport in transistors, conductance measurements are recommended. Fig. 2(a) shows the total conductance variation as a function of radical frequency at different polarization V_{gs}. As can be noticed, the conductance spectra shown certain typical properties such as at high-frequency increase and at low-frequency plateau. It is found that a change in the total conductivity slopes was noting in the high- and low-frequency areas. As also shown, two different regions are observed from conductance variation. At low-frequency, the detected plateau is frequency-independent and increase with the rise voltage. This clearly shows that the plateau is due to the long-distance movement of the charge carriers and correspond to dc conductance (σ_{dc}). The ac conductance, however, obeys a power law feature at high-frequency. In addition, the total conductance of AlGaN/GaN described as follows [23]:

$$\sigma (w) = \sigma_{dc} + w^s \tag{5}$$

where σ_{dc} is the dc conductance and w^s is the charge carriers transport characteristics. w is the angular frequency and s is the critical exponent refers to the conduction mechanism type in

structure. The parameter is determined from slopes of the linear parts of conductivity characteristics. The inset of Fig. 2b presents the conductivity characteristics at Vgs = 0V, as an example. Fig. 2b shows the critical exponent as a function of gate-to-source voltage. It is found that the critical exponent decrease going from 0.59 to 0.54 as a function of gate-source voltage rises. It should be noted that the critical exponent reduction is assigned to the barrier inhomogeneity, interface roughness and structural defects [24-28].

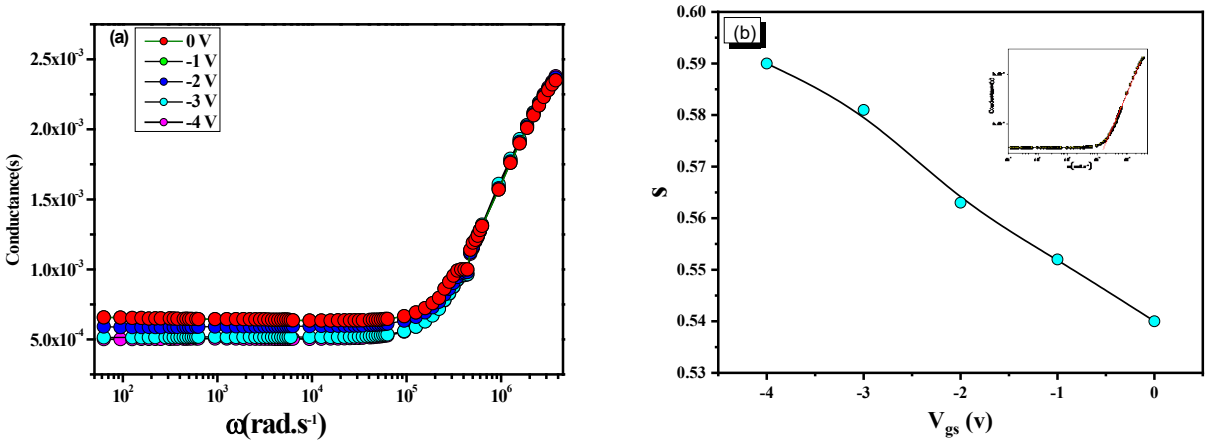

Fig. 2. (a) Frequency-dependent conductance of the AlGaN/GaN/Si HEMTs devices at different Bias voltage. (b) Variation of critical exponent. The inset represents the linear fit of conductance characteristics.

5. Impedance formalism

Fig. 3a shows the real part of complex impedance as a function of radical frequency at different bias voltage. It is found that the real part of impedance decreases with the frequency increase. As also shown, the Z' value decreases with deceasing gate-to-source voltage. Moreover, the real part of impedance shows the presence of constant region independent of frequency and decreases till a specific frequency. This behavior is due to the decrease in barrier height at AlGaN/GaN heterostructure [17]. Fig. 3b show the imaginary part of complex impedance as a function of radical frequency at different bias voltage. It is worth noticing that the imaginary part of impedance value increases initially with the frequency and exhibits a maximum before decreasing. However, the peak broadening is shifted to higher frequencies. This clearly that the peak broadening is slightly asymmetrical in character. This has led to a relaxation time process. The process caused by defects presence in AlGaN/GaN interface [17]. To more study the conductance characteristics, complex impedance plane are recommended. Fig. 3c shows the cole-cole plane plots of AlGaN/GaN HEMTs at different bias voltages. It is found that the presence of semi-circle not concentered on the real axis. As also shown, the diameter of the semi-circle decreases with decreasing applied bias voltages. It is worth noticing that the reduction of diameter is due to the conduction behavior thermally activated. However, to obtain the electric answer, impedance results were analyzed by the Z view software [29]. All spectra could excellently be fitted to the equivalent circuit. Fig. 3d shows the complex impedance spectrum at Vgs = 0V and the equivalent electrical circuit. It should be noted that the best fit for the impedance data included two parallel circuits (CPE_b/R_b and CPE_t/R_{2DEG}) and series resistance (R_s) connected in series, as illustrated in the inset of Fig. 3d. the parameters obtained for the electrical equivalent circuit are summarized in Table 1. The constant phase element (CPE) is expressed as follows [30]:

$$Z_{CPE} = \frac{1}{(2\pi f)^{\alpha}.\, Q_i} \tag{6}$$

where f is the frequency, α is the empirical exponent and Q_i is the interface charge. As can be seen, the CPE behavior include surface roughness, or non-uniform current distribution [30-33]. This

implies that the CPE is assigned to traps and 2DEG depletion in AlGaN/GaN heterointerface. The relationships between real (Z') and imaginary (Z'') part components of the impedance connected to the equivalent circuit can be expressed as [30]:

$$Z = Z' + j\,Z'' = R_s + \frac{1}{R_b^{-1} + (2\,j\,f)^{\alpha_b} Q_b} + \frac{1}{R_{2DEG}^{-1} + (2\,j\,f)^{\alpha_t} Q_t} \quad (7)$$

where R_s, R_b and R_{2DEG} are the resistance of ohmic contact, cap/barrier layers and 2DEG respectively. We report in Table 2 the values of the different resistance and CPE as deduced at different bias voltage. As can be seen, the electrical equivalent circuit parameters decreases with the voltage bias. This lowering is assigned to the decrease of electron mobility and trapping effects in devices.

Table 2. Electrical parameters of equivalent circuit deduced from impedance data for AlGaN/GaN/Si HEMTs devices at different bias voltages.

V	**R_s**	**R_b**	**CPE_b**	**α_b**	**R_{2DEG}**	**CPE_t**	**α_t**
0	390	626E9	7,05E-12	0,89476	563E9	7,83E-12	0,89619
-1	379	479E9	6,84E-12	0,92981	416E9	5,86E-12	0,92576
-2	374	204E9	5,97E-12	0,9342	141E9	3,51E-12	1,028
-3	366	128E9	4,09E-12	0,93992	65E9	2,98E-12	1,028
-4	364	101E9	3,44E-12	1,051	38E9	1,98E-12	1,046

Fig. 3e shows the variation of resistance as a function of gate-to-source voltage. It is found that the series resistance remains constant with the voltage bias. This implies that the leakage current remains much small in heterostructures. As also shown, bulk resistance (R_b and R_{2DEG}) increases with the increase of Vgs. However, bulk resistance values are higher than series resistance. The amount in bulk resistance is due to the occurrence of charge carrier in AlGaN/GaN heterointerface. More especially, a distribution of charge generation/recombination time constants is created by contribution of defect levels and trap states, in the band structure [30]. To determined trap distribution properties, adjusting bulk resistances values are recommended. Inset of Fig. 3e shows the bulk resistances as a function of bias voltage in log-log scale. It is worth noticing that the bulk resistance exhibits a linear variation. The slope values are determined from the linear fit of Ln (R – V). However, it is found that the slopes to be 0.97 and 0.99 of R_b and R_{2DEG} respectively. This clearly shows that the conductance of traps is due to an exponential trap distribution. This implies that the carriers may be trapped by impurities or defect levels or trap states [18].

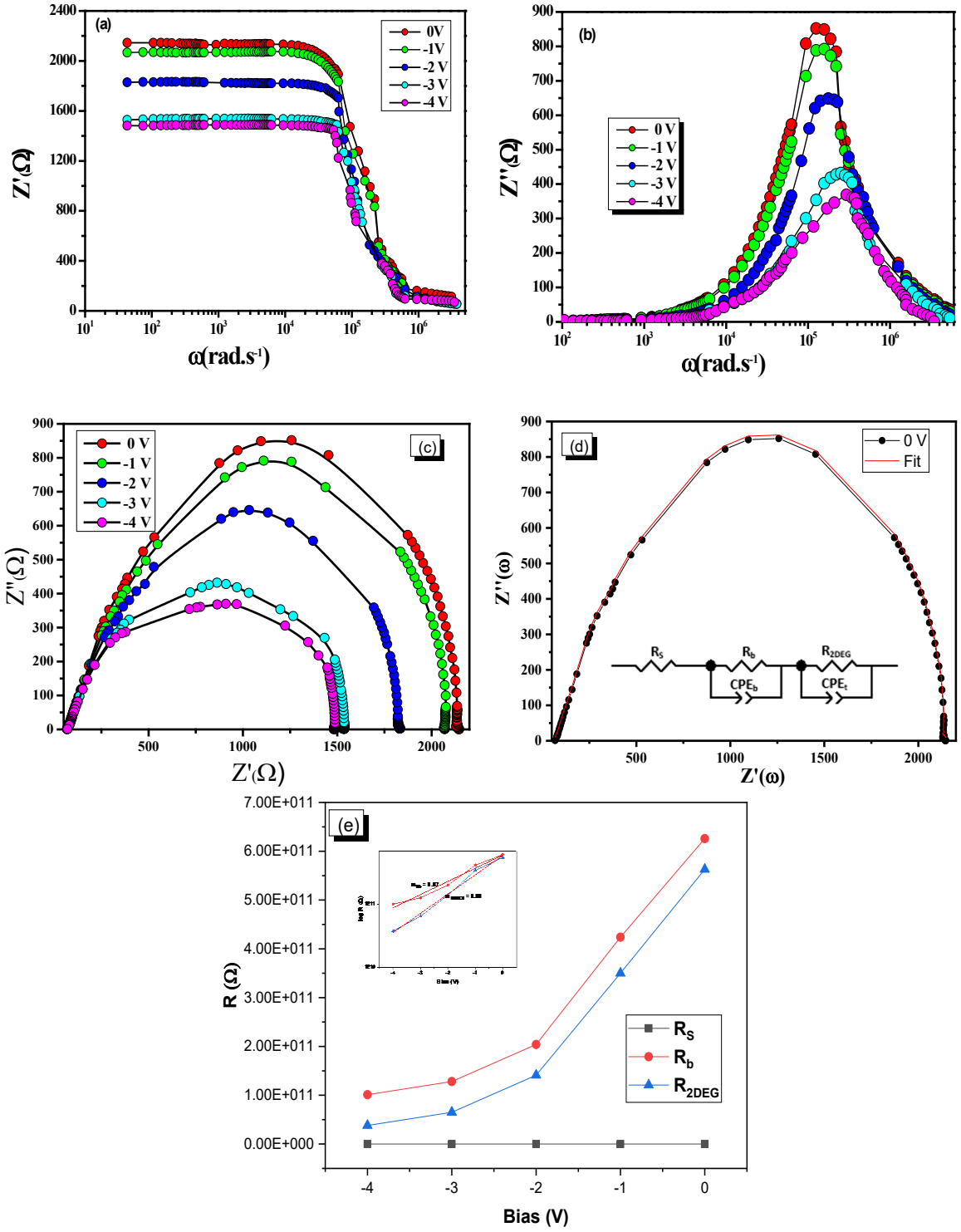

Fig. 3. Frequency-dependent of (a) the real part of impedance, (b) the imaginary part impedance, (c) Cole-cole plots of complex impedance, (d) Fits according to the equivalent circuit, (e) Variation of resistance. Inset the plot of log Rb and R_{2DEG} of the AlGaN/GaN/Si HEMTs devices.

6. Dielectric conductance analysis

Dielectric permittivity measurements have been performed on the sample. Fig.4 shows the permittivity imaginary parts (ε'') as a function of radical frequency. It should be noted that the permittivity imaginary decrease with the increase in frequency. As also shown, the permittivity

imaginary parts remains constant at higher frequency range. The latter behavior is due to dispersive of the (Mo/Au)/AlGaN/GaN Schottky barrier diode results from a strain relaxation in the AlGaN barrier layer under the (Mo/Au) Schottky gate [26,34-36]. It can be seen that the strain relaxation mechanism is enhanced due to collision between piezoelectric polarization dipoles and phonons [26]. The permittivity imaginary scaling as illustrated in the inset of Fig. 4. The scaling is determined from slope of the linear of ε''– w characteristics in a logarithmic scale. It is found that the scaling has been obtained around -1.01. This clearly shows that the relaxation mechanism will occur to cause permittivity falls [36]. Fig. 5 shows the dielectric loss as a function of radial frequency at different bias voltage. As can be seen, the loss tangent decreases with increases frequency. This implies that the colossal dielectric reponse and the barrier inhomogeneity is improved decrease in the dielectric loss. It should be noted that the dielectric loss rises sharply at lower frequencies. This proposal of explanation agrees will the relaxation mechanism results by decreasing permittivity. At higher frequencies, the dielectric loss, however, reaches constant values. It is found that the remains loss becomes thermally activated in conductance mechanism results from an increase of piezoelectric polarization. The remains loss is due to the occurrence of energy and transport conductivity. This has led to the strain relaxation in the AlGaN barrier layer [36].

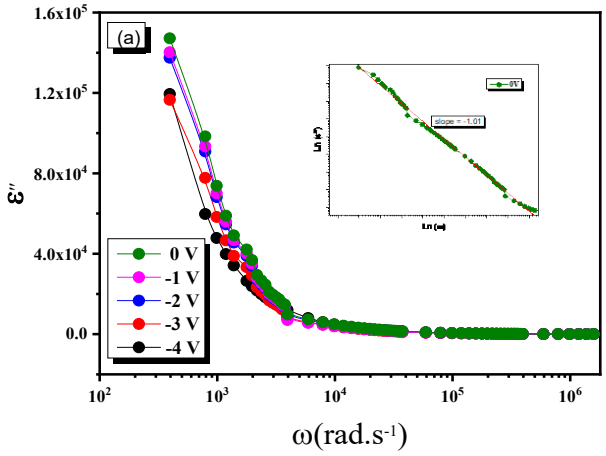

Fig. 4. Frequency-dependent Dielectric constant of the AlGaN/GaN/Si HEMTs devices at different bias voltage. The inset present the scaling of the ε''(ω).

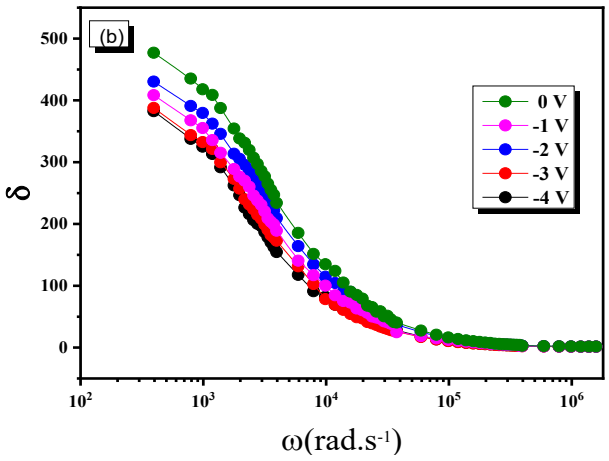

Fig. 5. Dielectric loss (tan δ) of the AlGaN/GaN/Si HEMTs devices at different bias voltage.

7. Complex modulus analysis

Complex modulus were also derived for AlGaN/GaN/Si HEMTs under dielectric measurements. From complex bulk properties, the conductance effect and the relaxation process in the devices [37]. The complex modulus is derived from the complex dielectric permittivity as follows [36,38]:

$$M^*(\omega) = \frac{1}{\varepsilon(\omega)} = M' + j\,M'' \tag{8}$$

where M' and M'' are the real and the imaginary electric modulus parts respectively.

Fig. 6a shows the real electric modulus parts as a function of radial frequency. It is found that the real modulus parts increases with frequency. The increase in the M'(ω), however, favors the dispersion tendency and relaxation process. This implies that the continuous dispersion is produced by the charge carriers mobility and the electric conduction in AlGaN/GaN heterointerface [36].

Fig. 6b shows the imaginary electric modulus parts as a function of radical frequency at different gate-to-source voltage. It can be seen that the imaginary modulus parts shows a two peaks. It is worth noticing that the two peaks are asymmetric peaks. Symmetric peaks are enhanced due to relaxation process in HEMT devices. This implies that the relaxation behavior is caused by thermally carrier generation activated at AlGaN/GaN heterostructure [36]. It is worth noticing that the existence of a deep levels and a structural defects in HEMTs. However, inhomogeneous Schottky barrier and conductance mechanism are assigned to the effect of traps on the device.

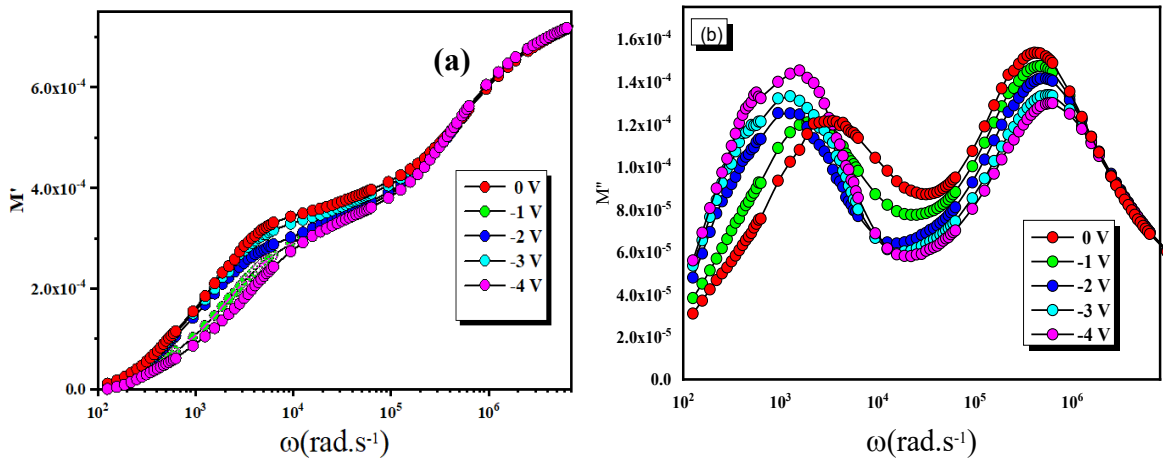

Fig. 6. (a) Real electric modulus, (b) Imaginary electric modulus of the AlGaN/GaN/Si HEMTs devices at different bias voltage.

8. DLTS experiments

DLTS technique is an experimental tool for studying electrically active defects in devices. Fig. 7 shows the DLTS signal of AlGaN/GaN/Si HEMT. It is found that the DLTS signal is composed of two peaks. The two deep electron traps named A1 and A2. The binding energies of these defects are evaluated from their signatures. Signatures of these defects are determined from the Arrhenius plot, as illustrated in the inset of Fig. 7. The physical parameters obtained for the electron traps are summarized in Table 3.

Table 3. Physical parameters of the electron traps in AlGaN/GaN/Si HEMT.

Electron traps	**A1**	**A2**
E_T (eV)	0.26	1.05
σ_n (cm^2)	$4.16.10^{-16}$	$5.42.10^{-15}$
N_T (cm^3)	$2.4.10^{15}$	$4.52.10^{15}$

The electron trap A1 is found to have an energy level at 0.26 eV, a capture cross section of $4.16.10^{-16}$ cm^2 and a concentration of $2.4.10^{15}$ cm^{-3}. It can be seen that this traps is similar to that reported by Mosbahi et al. [17,19,39] in a previous work for an MBE grown AlGaN/GaN/Si using DLTS and CDLTS. The same defect is also observed by Fang et al [40] for an HVPE grown n-GaN using DLTS. As an attempt of explanation, the electron trap A1 should to be a complex involving a pair of N- and Ga- vacancies. This trap might be a defect located at the AlGaN/GaN heterointerface.

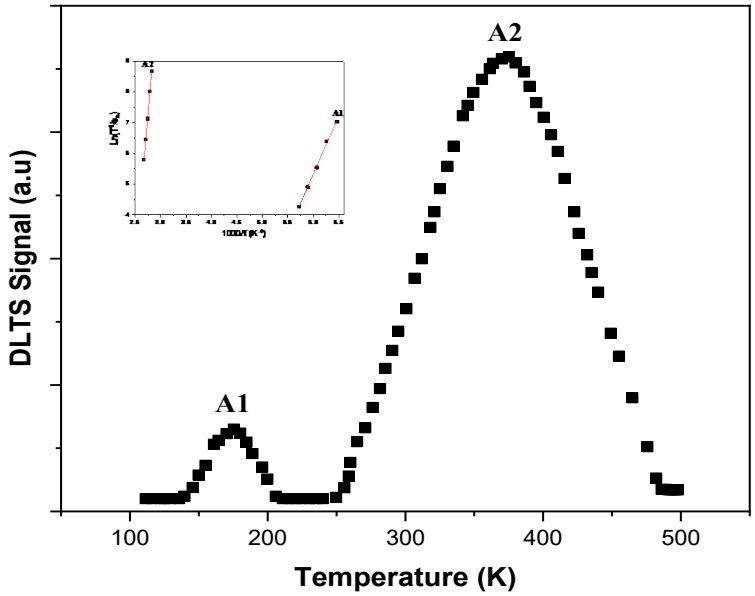

Fig. 7. DLTS spectra of the AlGaN/GaN/Si HEMTs. The inset illustrated the binding energies of Traps.

The deep center A2 is characterized by an ionization energy of 1.05 eV, a capture cross section of $5.42.10^{-15}$ cm^2 and a density $4.52.10^{15}$ cm^{-3}. It seems that this trap is observed in an AlGaN/GaN/Si HEMT for the first time to our knowledge. The nature of such a defect remains an open question.

9. Conclusion

In the present work, we have investigated the transport properties of AlGaN/GaN/Si HEMTs. The electrical and dielectrical behavior of the devices is characterized by using DC, G(ω), impedance, modulus and DLTS measurements. In fact, the DC and conductance behaviors shows a number of anomalies assigned to deep levels. As for the complex impedance data, they relevated that the cole-cole plane plots were fitted by an appropriate equivalent circuit. Moreover, dielectric studies enhaced that the relaxation behavior is caused by the presence of deep levels in devices. Traps in AlGaN/GaN/Si HEMTs were measured by DLTS technique. These traps are responsible for trapping/detrapping phenomena in heterostructure.

Acknowledgements

The authors extend their appreciation to the Deanship of Scientific Research at King Khalid University for funding this work through Research Groups Program under grant number (RGP.1/24/44).

References

[1] P. Kordoš, G. Heidelberger, J. Bernát, A. Fox, M. Marso, H. Lüth, Appl. Phys. Lett. 87, 143501 (2005); https://doi.org/10.1063/1.2058206

[2] H. Kambayashi, Y. Satoh, S. Ootomo, T. Kokawa, T. Nomura, S. Kato, T.-S. P. Chow, Solid State Electron. 54, 660 (2010); https://doi.org/10.1016/j.sse.2010.01.001

[3] Y. Murase, K. Asano, I. Takenaka, Y. Ando, H. Takahashi, C. Sasaoka, IEEE Electron Device Lett. 35, 524 (2014); https://doi.org/10.1109/LED.2014.2308313

[4] T. Hashizume, S. Anantathanasarn, N. Negoro, E. Sano, H. Hasegawa, K. Kumakura, T. Makimoto, Jpn. J. Appl. Phys. 43, L777 (2004); https://doi.org/10.1143/JJAP.43.L777

[5] H. Morkoç, Handbook of Nitride Semiconductors and Devices, vols. IeIII, Wiley-VCH, Berlin, 2008; https://doi.org/10.1002/9783527628445

[6] O. Ambacher, J. Smart, J.R. Shealy, N.G. Weimann, K. Chu, M. Murphy, W.J. Schaff, L.F. Eastmann, R. Dimitrov, L. Wittmer, M. Stutzmann, W. Rieger, J. Hilsenbeck, J. Appl. Phys. 85, 3222 (1999); https://doi.org/10.1063/1.369664

[7] Guacci, M.; Anderson, J.A.; Pally, K.L.; Bortis, D.; Kolar,J.W.; Kasper, M.J.; Deboy, G. IEEE J. Emerg. Sel. Top. Power Electron. 8, 2238 (2020); https://doi.org/10.1109/JESTPE.2019.2944268

[8] Jafari, A.; Nikoo, M.S.; Perera, N.; Yildirim, H.K.; Karakaya, F.; Soleimanzadeh, R.; Matioli, E. IEEE Trans. Power Electron. 35, 12595 (2020); https://doi.org/10.1109/TPEL.2020.2990628

[9] M. Gassoumi, Semiconductors. 54, 129647 (2020); https://doi.org/10.1134/S1063782620100127

[10] I.P. Smorchkova, L. Chen, T. Mates, L. Shen, S. Heikman, B. Moran, S. Keller, S.P. DenBaars, J.S. Spech, U.K. Mishra, J. Appl. Phys. 90, 5196 (2001); https://doi.org/10.1063/1.1412273

[11] Y. Cao, D. Jena, Appl. Phys. Lett. 90, 182112 (2007); https://doi.org/10.1063/1.2736207

[12] S.B. Lisesivdin, A. Yildiz,M. Kasap, Opt. Adv.Mater.-Rapid Commun. 1 (2007) 467.

[13] R. Vetury, N. Q. Zhang, S. Keller, U. K. Mishra, IEEE Trans. Electron Devices 48, 560 (2001); https://doi.org/10.1109/16.906451

[14] Y. -R. Wu, J. Singh, J. Appl. Phys. 101, 113712 (2007).

[15] C. Rivera, E. Munoz, Appl. Phys. Lett. 94, 053501 (2009).

[16] G. Meneghesso, G. Verzellesi, R. Pierobon, F. Rampazzo, A. Chini, U. K. Mishra, C. Canali, E. Zanoni, IEEE Trans. Electron Devices 51, 1554 (2004); https://doi.org/10.1109/TED.2004.835025

[17] H. Mosbahi, M. Gassoumi, I. Saidi, H. Mejri, C. Gaquière, M.A. Zaidi, H. Maaref, Current Applied Physics. 13, 1359 (2013); https://doi.org/10.1016/j.cap.2013.04.003

[18] H. Mosbahi, M. Gassoumi, M. A. Zaidi, Silicon. 14, 3899 (2022); https://doi.org/10.1007/s12633-021-01164-7

[19] Mosbahi, H., Gassoumi, M., Guesmi, A., Ben Hamadi, N., Zaidi, M.A., Journal of Ovonic Research, 18, 159 (2022); https://doi.org/10.15251/JOR.2022.182.159

[20] T. Okino, M. Ochiai, Y. Ohno, S. Kishimoto, K. Maezawa, T. Mizutani, IEEE Electron Device Lett. 25, 523 (2004); https://doi.org/10.1109/LED.2004.832788

[21] E. J. Miller, X. Z. Dang, H. H. Wieder, J. Appl. Phys. 87, 8070 (2000); https://doi.org/10.1063/1.373499

[22] S. Quan, Y. Hao, X. H. Ma, Chin. Phys. B 20, 018101 (2011); https://doi.org/10.1088/1674-1056/20/1/018101

[23] A. K. Jonscher, Thin Solid Films 1, 213 (1967); https://doi.org/10.1016/0040-6090(67)90004-1

[24] S. Zhu, R. L. Van Meirhaeghe, S. Forment, G. P. Ru, X. P. Qu, B. Z. Li, Solid-State Electron. 48, 1205 (2004); https://doi.org/10.1016/j.sse.2004.02.006

[25] Y. G. Chen, M. Ogura, H. Okushi, Appl. Phys. Lett. 82, 4367 (2003); https://doi.org/10.1063/1.1583868

[26] Y. Dawei, W. Fuxue, Z. Zhaomin, C. Jianmin, G. Xiaofeng, J. Semicond. 34, 014003-1 (2013); https://doi.org/10.1088/1674-4926/34/1/014003

[27] S. Zeyrek, Ş. Altındal, H. Yüzer, M. M. Bülbül, Appl. Surf. Sci. 252, 2999 (2006); https://doi.org/10.1016/j.apsusc.2005.05.008

[28] Ş. Altındal, S. Karadeniz, N. Tuğluoğlu, A. Tataroğlu, Solid-State Electron. 47, 1847 (2003); https://doi.org/10.1016/S0038-1101(03)00182-5

[29] D. Johnson, ZView: A Software Program for IES Analysis, Version 2.8, Scribner Associates, Inc., Southern Pines, NC, 2002.

[30] M. Donahue, B. Lübbers, M. Kittler, P. Mai, A. Schober, Appl. Phys. Lett. 102, 141607 (2013); https://doi.org/10.1063/1.4801643

[31] K. S. Cole, R. H. Cole, J. Chem. Phys. 9, 341 (1941); https://doi.org/10.1063/1.1750906

[32] J. R. Macdonald, W. R. Kenan, Impedance Spectroscopy : Emphasizing Solid Materials and Systems, Wiley Interscience, New York, 1987.

[33] G.J. Brug, A. L. G. Van Den Eeden, M. Sluyters-Rehbach, J. H. Sluyters, J. Electroanal. Chem. 176, 275 (1984); https://doi.org/10.1016/S0022-0728(84)80324-1

[34] B. I. Bleaney, B. Bleaney, Electricity and magnetism. 3rd ed. London : Oxford University Press, 1976.

[35] F. S. Xue, Research & Progress of SSE. 27, 457 (2007).

[36] Mosbahi, H., Gassoumi, M., Bchetnia, A., Zaidi, M.A., Silicon 14, 7417 (2022); https://doi.org/10.1007/s12633-021-01486-6

[37] S. EL. Kossi, F. I. H. Rhouma, J. Dhahri, K. Khirouni, Physica B. 440, 118 (2014).

[38] C. Leon, P. Lunkenheimer, K.L. Ngai, Phys. Rev. B. 64, 184304 (2001); https://doi.org/10.1103/PhysRevB.64.184304

[39] H. Mosbahi, M. Gassoumi, M. Charfeddine, M.A. Zaidi, C. Gaquiere, H. Maaref, J. Optoelectron. Adv. M. **12**(11), 2190 (2010).

[40] Z.Q. Fang, D.C. Look, J. Jasinski, M. Benamara, Z. LilientalWeber, R.J. Molnar, Appl. Phys. Lett. 7, 332 (2001); https://doi.org/10.1063/1.1338970